DOI: 10.13009/EUCASS2019-118

Numerical Simulation of BTI Broadband Noise Reduction with Wavy Leading Edge for Sweep Blade*

QIAO Weiyang[1], DUAN Wenhua[2], GUO Xin[3], CHEN Weijie[4] and TONG Fan[5]
School of Power and Energy, Northwestern Polytechnical University, Xi'an 710072, China

A hybrid LES/FW-H simulation is performed to investigate the leading-edge broadband noise reduction of a sweep blade with Wavy Leading Edge(WLE) configuration. The noise radiation from the sweep blade leading-edge is generated by the interaction of the blade and incoming anisotropic turbulence (Blade-Turbulence Interaction noise, BTI noise) which is produced by a rod whose wake impinges onto the downstream blade. The incoming flow velocity is 40m/s and the corresponding blade chord based and rod diameter based Reynolds number is about 400,000 and 26,000 respectively. The far field acoustic field is predicted using the FW-H acoustic analogy method which has been validated against the experimental results. A Straight leading Edge(SLE) blade and a WLE blade are simulated in the study. Results show that the WLE can substantially reduce BTI noise when the incoming turbulence is anisotropic, and can mitigate noise radiation at all the azimuthal angles without significantly changing the noise directivity. As expected, the reduction of the sound pressure level of BTI noise for three-dimensional swept blade with WLE configuration is not as significant as that of two-dimensional blade. The OASPL of the BTI noise reduction associated with the WLE is approximately 2.4~3.4dB. The underlying noise reduction mechanism is then analyzed in detail. It is found that WLE can significantly change the flow pattern around the leading edge of swept blade. The present results show that the pressure fluctuation around the blade leading edge and the unsteady load on the swept blade were significantly reduced with the using of WLE configuration.

***Keywords*: Broadband noise; Large eddy simulation; Wavy leading edge; Sweep blade; Noise reduction mechanism**

1 Introduction

The reduction of the turbulence broadband noise from the trailing-edge (TE) and leading-edge(LE) of wing or the turbomachinery blade is nowadays an important industrial need and probably one of the most challenging issues in aero-acoustics. Especially, the Blade-Turbulence Interaction(BTI) noise which from the interaction between the incoming turbulence and blade leading edge is a significant contributor to the noise of turbofan, wind turbines, ventilation systems, high-lift devices, propellers, and so on. It has been found that the BTI noise can be the dominant source when the incoming turbulence intensity is sufficiently high[1], which is often the case at the leading edge (LE) of outlet guide vanes in modern high-bypass-ratio turbofan engines.

In order to achieve the dream of ultra-quiet flight in the future, "learning from nature" which is the core of the noise control using bionic methods, has received unprecedented attention and been investigated extensively. Learning from nature can help to provide new aerodynamic noise control ideas, and has become a new vibrant aerodynamic noise control field. The wavy or serrated leading edge (Wavy Leading Edge, WLE) was originally

* Project Grant No. 51776174 supported by National Natural Science Foundation of China, the National Special Research Project in Aeroengine in China, and the International cooperation project (IMAGE) in aeronautics between China and European Union (Grant Agreement 688971-IMAGE).
[1] Professor, Northwestern Polytechnical University, Xi'an, China,710072,Qiaowy@nwpu.edu.cn
[2] PhD Student, Northwestern Polytechnical University, Xi'an China,710072, duanwenhua@mail.nwpu.edu.cn
[3] Ms Student, Northwestern Polytechnical University, Xi'an China,710072, guoxin_ms@mail.nwpu.edu.cn
4 PhD Student, Northwestern Polytechnical University,Xi'an China,710072, cwj@mail.nwpu.edu.cn
[5] PhD Student, Northwestern Polytechnical University,Xi'an China,710072, nwputongfan@163.com

DOI: 10.13009/EUCASS2019-118

bioinspired by owl serrations leading-edge wings and Humpback whale flippers, has been identified as a lift-enhancing, drag-reducing and noise reducing modification[2-5]. WLE has become the focus of much research to explore their benefits in terms of improved aerodynamic performance and/or reducing noise. Most of the studies demonstrate that the WLE can delay the stall occurrence, increase post-stall lift, decrease post-stall drag, and reduce the laminar separation bubble, whereas it may degrade the pre-stall performance [6–18].

In addition to the aerodynamic aspects, many studies have focused on BTI noise reduction with the WLE in recent years[19-36]. Clair et al.[19] experimentally and numerically investigated the effects of WLE on the airfoil-turbulence interaction noise, reporting a noise reduction of 3-4dB. Lau et al.[20] numerically investigated the effects of WLE on the airfoil-gust interaction noise(AGI), finding that the ratio of the WLE peak-to-valley amplitude (A) to the longitudinal wavelength of the incident gust (λg) was an important factor in reducing AGI noise. Kim et al.[24] conducted a numerical investigation into the noise reduction mechanisms of WLE, obtaining valuable results. Mathews and Peake[25] and Lyu et al.[26] also performed theoretical analyses of noise reduction using WLE. Chaitanya et al.[27] conducted a detailed parametric study of the sensitivity of noise reduction effects to the amplitude and wavelength of the leading-edge serrations of flat plates and a NACA-65(12)10 airfoil. The influence of the turbulence integral length scale is also studied. Biedermann et al.[28] proposed a statistical-empirical model to predict the noise generated by WLE airfoils. Turner and Kim[29] numerically investigated the aeroacoustic source mechanisms of WLE on a flat plate, identifying a system of horseshoe-like secondary vortices developing around the WLE. Aguilera et al. [30] investigated the interaction of anisotropic turbulence with a WLE NACA 0012 airfoil by means of computational aeroacoustic simulations (CAA). Reboul et al. [31] performed a CAA prediction of the broadband noise reduction effects of a serrated OGV using synthetic turbulence. A reduction in overall sound power level of 1.9 dB was reported [31]. More recently, a series of experimental and numerical simulation studies on the broadband noise reduction with WLE was carried out by present authors in Northwest Polytechnic University(NPU) [33-36].

Despite the rapid growth in this field, the understanding of the noise reduction mechanisms associated with wavy leading edge is still underdeveloped[37]. For the above most research works, most of the studies have been focused on 2-dimensional airfoils and flat plates with 2-dimensional flow. and most previous studies have used homogeneous isotropic and grid generated turbulence. To the authors' knowledge, real fan noise reduction using wavy leading-edges has only been reported recently by Tong et al.[36] and Reboul et al. [38](in fact, the simplified approximate two-dimensional flow simulation method is still used in these study[36]), and the investigation of lead-edge noise reduction with incoming anisotropic turbulence has only been reported recently by Chen et al.[33,34] and Tong et al [35]. It is well known that the flow around blade of turbomachinery presents a strong three-dimensional flow characteristics. It could be expected that the flow and acoustic mechanism of the WLE in turbomachinery are more sophisticated than that in the already existing theory with the supposing of 2-dimensional flow airfoil. In the current work, a swept blade which model the three-dimensional flow characteristics around blade is used to study the BTI noise reduction mechanism of WLE configuration. The incoming anisotropic turbulence was generated using a rod wake which is placed before the swept blade.

The organization of the paper is as follows. In Sec. 2, the validated hybrid computational aeroacoustics methodology and the parameters of the WLE model are described. Then the numerical model and numerical simulation setup are presented in Section 3. In Sec. 4, the aerodynamic effects and noise reduction effects of WLE on the swept blade are presented. The noise reduction mechanisms of the WLE are elaborated in detail in Sec. 5. Finally, some conclusions are drawn in Sec. 6.

2 Numerical Methodology

In this paper, a validated the hybrid computational fluid dynamics (CFD)/acoustic analogy method is used to calculate swept blade BTI noise[39,33-35]. First, the noise sources of the swept blade, most importantly, the pressure fluctuations on the blade surfaces, are obtained using the CFD method. Next, the pressure fluctuations are transformed into noise sources in the frequency domain using Fast Fourier Transform(FFT). Finally, the noise sources in the frequency domain are coupled with the FW-H equations to obtain the sound power level generated by the BTI.

2.1. Numerical method for flow field

The broadband nature of the noise sources for BTI noise should be captured by the simulation in the current paper, as broadband noise which generally requires direct numerical simulation (DNS) or LES. LES is used to compute the flow field in this paper.

DOI: 10.13009/EUCASS2019-118

In LES, the large scales of the flow and small scales of the flow are treated differently according to their different characteristics. Generally speaking, large scales of the flow contain the main part of the total fluctuating kinetic energy and characterize the flow. They drive the physical mechanisms of the flow. At the same time, the large scales of the flow are sensitive to the boundary conditions and are anisotropic.[40] In contrast, small scales of the flow contain only a few percent of the total kinetic energy and have weak influence on the mean fluid motions. Their main function is viscous dissipation. In LES, the large three-dimensional unsteady turbulent motions are directly solved, whereas the effects of the smaller-scale motions are modelled by the subgrid-scale (SGS) stress model.

In the current paper, the commercial available solver CFX[41] is used to calculate the flow field and the dynamic Smagorinsky-Lilly model[42] is used whose model coefficient can adjust automatically to the flow type according to the information contained in the resolved turbulent velocity field. This model has demonstrated satisfactory results by Winkler[43] and the authors' previous study[39].

2.2. Far field noise prediction

The far field noise prediction method is based on Goldstein's generalized Lighthill equation[44]. The fundamental equation governing the generation of sound in the presence of solid boundaries is presented below[44]

$$c_0^2\rho'(\vec{\mathbf{x}},t)=\int_{-T}^{T}\int_{A(\tau)}\rho_0 V_N'\frac{DG}{D\tau}dA(\vec{\mathbf{y}})d\tau + \int_{-T}^{T}\int_{A(\tau)}\boldsymbol{f}_i\frac{\partial G}{\partial y_i}dA(\vec{\mathbf{y}})d\tau+\int_{-T}^{T}\int_{v(\tau)}\boldsymbol{T}_{ij}'\frac{\partial^2 G}{\partial y_i\partial y_j}d\vec{\mathbf{y}}d\tau \tag{1}$$

where c_0 is the ambient speed of sound and ρ' is the acoustic density disturbance. At sufficient distance from the source, $c_0^2\rho'$ is equal to the acoustic pressure p'. τ is the source time (retarded time). V_N' is the velocity of the surface normal to itself relative to the fluid.

When the incoming flow Mach number is small and the solid surface keeps statistic, which is often the case in the acoustic wind tunnel experiments, the first and third term on the right hand of Eq.(1) can be ignored. Therefore, Eq.(1) can be simplified as

$$p'(\vec{\mathbf{x}},t)=\int_{-T}^{T}\int_{A(\tau)}\boldsymbol{f}_i\frac{\partial G}{\partial y_i}dA(\vec{\mathbf{y}})d\tau \tag{2}$$

where G is the free space, moving medium, time dependent Green function

$$G=\frac{\delta(t-\tau-\sigma/c_0)}{4\pi S} \tag{3}$$

S is the amplitude radius

$$S=\sqrt{(x_1-y_1)^2+\beta^2\left[(x_2-y_2)^2+(x_3-y_3)^2\right]} \tag{4}$$

and σ is the phase radius with $\beta^2=1-M^2$

$$\sigma=\frac{M(x_1-y_1)+S}{\beta^2} \tag{5}$$

$$M=U_0/c_0 \tag{6}$$

More Details about the noise prediction method can be seen in Ref 39. For clarity, only the final expression for the far field acoustic pressure is presented herein as follows[39].

3. Model and numerical set up

3.1. Model

The swept blade with sweep angle of 30 degrees and constructed by NACA0012 airfoil was numerical investigated in this study. The chord of the swept blade is of 150mm and the span is of 300mm.

DOI: 10.13009/EUCASS2019-118

In order to investigate the effect of WLE on the blade-turbulence interaction noise(BTI), the swept blade with modified leading edges, i.e. wavy leading edges, is designed as shown in figure1. The wavy peak, middle, and valley locations are also depicted in this figure. The averaged Leading Edge(LE) line of the WLE(defined as Wavy LE in figure 1) coincides with the LE of the Straight Leading Edge(SLE, defined as Baseline LE in figure 1) case so that the mean chord length and the wetted area of the wavy sept blade are maintained constant as that of SLE blade. The WLE blade in the form of sinusoidal profile with amplitude A, wavelength W, and mean chord length c is shown in Fig. 1(a). It should be noted that the wave shape in figure 1 is obtained by projecting a sinusoidal line with amplitude A and wavelength W perpendicular to the flow direction to the blade spanwise direction. Therefore, the wavelength W is perpendicular to the direction of the inflow. The symmetrical lines of the sinusoidal profile passing through the crest and valley points of the wave are parallel to the flow direction of the airflow. The chord length of the WLE blade versus spanwise coordinate z is of the form

$$c(z) = \bar{c} + \frac{A}{2} \cdot \cos\left(\frac{2\pi z}{W}\right) \tag{1}$$

The coordinates of the baseline swept blade are modified in the nose region according to Eq. (2). The x coordinates near the nose are stretched or contracted in line with the spanwise chord length of the WLE blade, while the rear coordinates are unchanged.

$$\begin{cases} x' = \begin{cases} \dfrac{x}{x_{max}}\left[x_{max} + (c(z) - \bar{c})\right] - \left[c(z) - \bar{c}\right] + z \cdot \tan\Lambda, & x < x_{max} \\ x + z \cdot \tan\Lambda, & x \geq x_{max} \end{cases} \\ y' = y \end{cases} \tag{2}$$

where the parameters with superscript ‘ refer to the modified blade. Subscript max refers to the location of the maximum thickness. Λ is the sweep angle of blade.

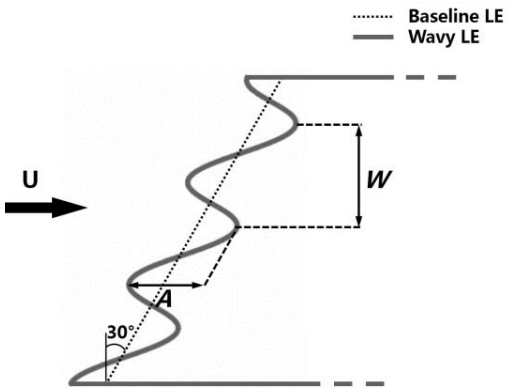

(a)The definition of wavy leading edge for swept blade

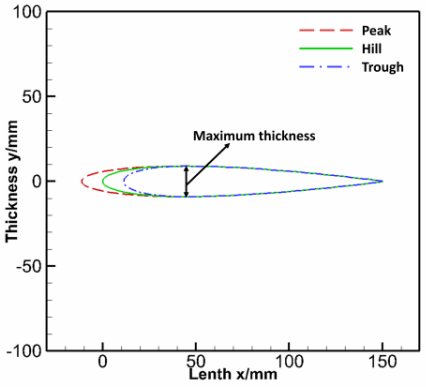

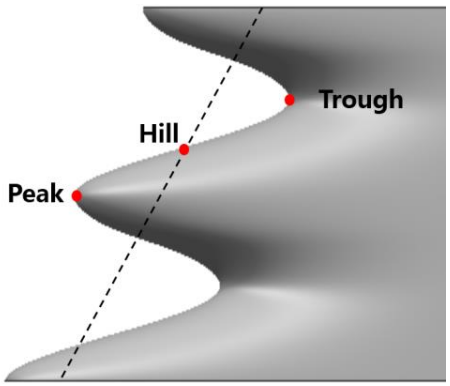

(b)The section profile of wavy LE (c) the typical position of wavy LE

Fig. 1 Sketch of wavy leading edge of swept blade

3.2. Flow Configuration

The present numerical simulation is based on the rod - blade flow configuration with SLE and WLE swept blades located downstream of the rod, to investigate the effect of the WLE on the BTI noise. The flow behand of rod is often used to simulate the wake turbulence of turbomachinery blade. The downstream of rod is composed of non-isotropic turbulence dominated by Karman vortex street, which is very similar to the phenomena observed in turbomachinery. The wavy blade which is with wave amplitude A is 15% of the average chord length, the wavelength W is 10% of the average chord length, and the sweep angle is 30 degrees is numerical simulated.

As shown in figure 2, an cylinder with the same sweep angle of 30 degree as that of swept blade is placed upstream of swept blade to model the interaction between turbulence and swept blade. The cross-section diameter of the cylinder is d=10 mm, and is placed at L=100 mm upstream of the leading edge of the swept blade(about the 0.67 blade chord). The x-axis is in the direction of flow direction, the y-axis is in the direction of transverse direction, the z-axis is in the spanwise direction. The boundary of the flow field includes the inflow boundary (solid line part) and the exit boundary (dotted line part). The outer flow field is a circular region with the center point at the maximum thickness of the blade as the center and the radius is 20 times blade chord(R=20c). Considering the requirement of mesh refinement for the WLE case and the limited computation resources, a reduced span length of twice the blade chord (2c) is chosen in the current study to reduce the mesh size and computation time, and this span length is corresponding to two wavelengths of WLE.

The computational domain also sweep 30 degrees in the spanwise direction, which ensures that the geometrical structures of the two ends in span direction are identical. It is convenient to impose periodic translation interface at the positions of the spreading surfaces, so that the whole model can be regarded as extending to infinite length. In this way, it is easy to impose periodic translation interface at the positions of both ends of the spanwise direction. This choice is consistent with some of the previous studies[32-35]. When it comes to the boundary condition in the spanwise direction, slip conditions, symmetry conditions, and periodic conditions have been used in the literature. For the free-slip conditions, the velocity components parallel to the wall have finite values (which are computed), but the velocity normal to the wall and the wall shear stress are both set to zero. The slip condition only affects the vicinity of the boundary. The symmetry condition imposes constraints that mirror the flow on either side of it. The velocity normal to the symmetry boundary and the scalar variable gradients normal to the boundary are both set to zero. For the periodic conditions, all the flow field quantities of the two periodic planes are fully correlated, which means that the periodic conditions impose more constraints on the flow field. It was reported by Boudet et al.[45] that the slip condition was physically more relevant and allowed a better comparison with the experiment. Meanwhile, it was pointed out by Kato et al.[46] that the slip condition might also be controversial. The periodic boundary condition is imposed in the spanwise direction in the present study because it was widely used in the literature and has been proven to be an appropriate choice. The previous numerical investigations are not further discussed in detail, because our main purpose in the current work is to explore the noise reduction effects and mechanisms of the WLE.

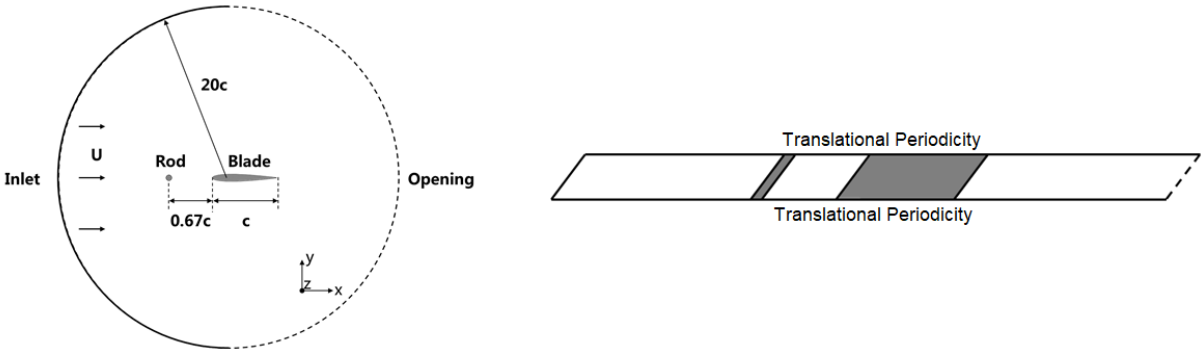

(a) y-direction (b) y-direction

Fig. 2 Sketch of the computational domain

3.3. computation grids

The sketch of computational mesh around the rod and airfoil is shown in figure 3. The far-field of inlet flow and exit flow boundary is circular. The four-layer "O" grid topology is adopted to control the boundary area and the area

DOI: 10.13009/EUCASS2019-118

near the blade surface separately. In order to reduce the boundary reflection, the mesh in the far-field boundary area far from the blade and cylinder is stretched. In order to obtain the flow details better, the meshes near the blade and the cylindrical wall are refined.

The grid around the blade is shown in Fig. 3(b). A "C" grid topology is adopted near the blade surface. In order to control the mesh quality conveniently, a three-layer grid control curve is generated outside the blade, which makes the grid near the blade surface three-layer nested structure. The "O" grid structure around the cylinder is also nested with three layers of grid. In order to capture Karman Vortex Street more precisely, the maximum mesh spacing in the wake region of the cylinder is 0.45 mm, the maximum mesh spacing on the blade surface is 0.88 mm, the number of nodes around the blade is about 500, the number of nodes around the cylinder is about 240, the number of nodes extending to the grid is 49, and the number of nodes in the grid is about 5.4 million.

For WLE blade, the grid is refined in the spreading direction, and the number of grid nodes in the wake region of the cylinder is increased to ensure that the maximum grid spacing is still 0.45 mm. In order to capture the flow field information at the wavy leading edge more carefully and ensure the quality of the grid, the number of the grid nodes in span direction increased to 53, and the total number of nodes increased to 6.4 million. Figure 3 (c) shows the surface grid of the wave front blade.

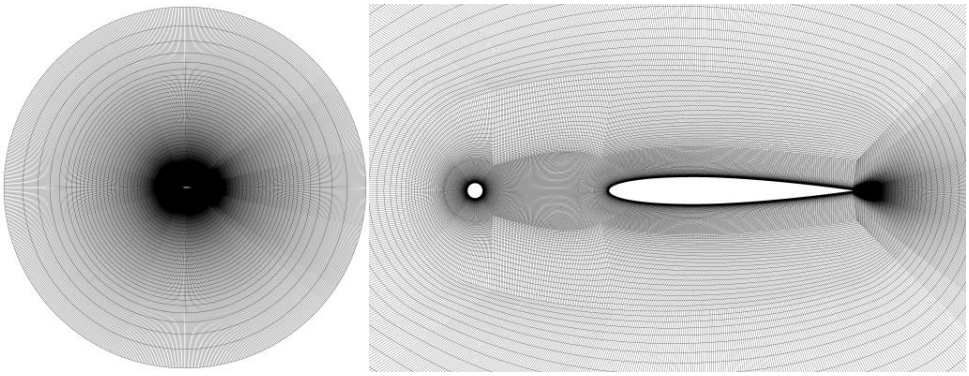

(a) grids in far-filed (b)grids around blade and rod

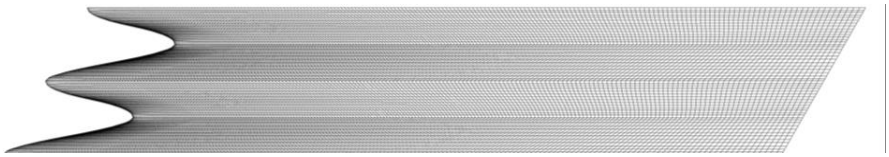

(c)grids in the wavy leading edge

Fig.3 computation mesh

Fig. 1 shows the dimensionless grid size distribution along the streamwise direction and wall normal direction. It can be seen that wall normal mesh dimensionless size $\Delta y+$ is less than 1 and streamwise mesh dimensionless size $\Delta x+$ is less than 100 over most of the airfoil surface, which is in accordance to the suggestion by Wagner[40]. Moreover, the authors' previous simulation for a similar configuration[39] indicates that the grid size in x-y plane is sufficient.

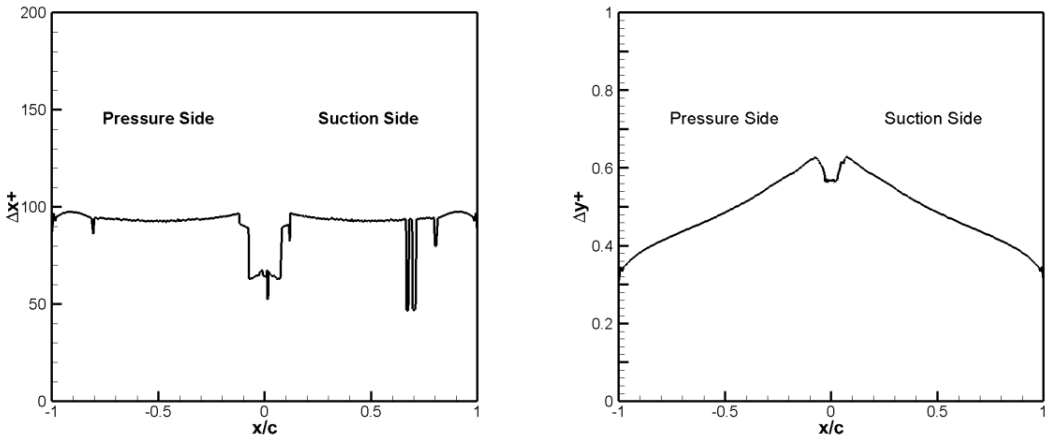

(a) Δx+ (b) Δy+

Fig. 1 Dimensionless grid size distribution

3.4. Numerical set up and boundary conditions

The boundary conditions used in this study are set as follows: the inlet boundary is set as the velocity inlet, the flow direction is the x-axis positive direction, and the flow velocity is U=40 m/s, and the Reynolds number based on the blade chord length is Re=4*10^5. The outlet boundary is set as Opening boundary, the outlet static pressure is standard atmospheric pressure P=101325 Pa, and the temperature is T=288 K. The boundary on both sides of the span direction is set as the periodic boundary of translation. The surface of cylinder and blade is set as non-slip adiabatic wall.

Firstly, the steady RANS calculation is used, and the steady RANS computation results are used as the initial field for the LES calculation. After the convergence of the LES calculation, the required flow field information is further promoted and counted, and the far-field noise information is obtained by using the FW-H method with the pressure fluctuation on the blade surface. The plane of far-field acoustic receiving points is on the middle span plane as shown in figure 5. The receiving points are centered at the center of the maximum thickness of the blade and the circle with radius of 2m. The blade chord direction is 0 azimuth angle, and the azimuth angle difference between the receiving points is 10 and the total number of receiving points is 36.

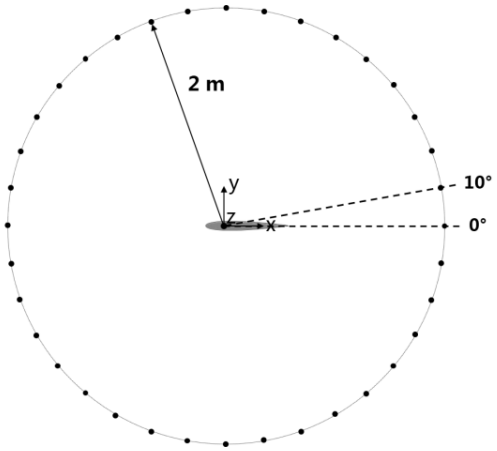

Fig. 5 The distribution of sound receiving points in far-field

4. The aerodynamic effects and noise reduction of WLE on the swept blade

4.1. Aerodynamic performance of the swept blade with WLE

The lift coefficient C_L , drag coefficient C_D and spanwise force coefficient C_S are used to evaluate aerodynamic performance of swept blade, which are defined as

DOI: 10.13009/EUCASS2019-118

$$C_L = \frac{F_y}{\frac{1}{2}\rho_0 U^2 S} \tag{3}$$

$$C_D = \frac{F_x}{\frac{1}{2}\rho_0 U^2 S} \tag{4}$$

$$C_S = \frac{F_z}{\frac{1}{2}\rho_0 U^2 S} \tag{5}$$

where F_x, F_y and F_z is the force on the airfoil in x, y and z direction and S is the blade projected area.

The time history of lift coefficient for SLE swept blade and WLE swept are shown in figure 6. It can be seen from figure 6 that WLE can significantly reduce lift coefficient fluctuation while the mean lift coefficient does not vary too much. Because the blade studied in this paper is NACA0012 symmetrical airfoil, the lift coefficient fluctuates near the zero value. In order to quantify the difference more clearly, the mean and root mean square (RMS) value of the lift, drag coefficient and spanwise force coefficient are presented in Fig. 7(a), Fig. 7(b), Fig. 7(c) respectively.

As can be seen from Figure 7, for swept blades, the WLE can slightly affect the lift coefficient of the blades, while reducing the average drag coefficient of the blades by 46.7%. This shows that the wavy leading edge can reduce the drag. At the same time, the fluctuation of lift coefficient and drag coefficient can be reduced by 21.2% and 8.3% respectively. The flow noise radiated from the flow around the blade usually consists of lift noise and drag noise due to the fluctuation of the lift and drag on the blade. The reduction of lift coefficient and drag coefficient fluctuation indicates that the structure of WLE can reduce the aerodynamic noise of blade. However, the existence of WLE can greatly increase the spanwise force on the blade, increasing by 247.1%, and at the same time will increase the root mean square value of the spanwise force by about 52.4%.

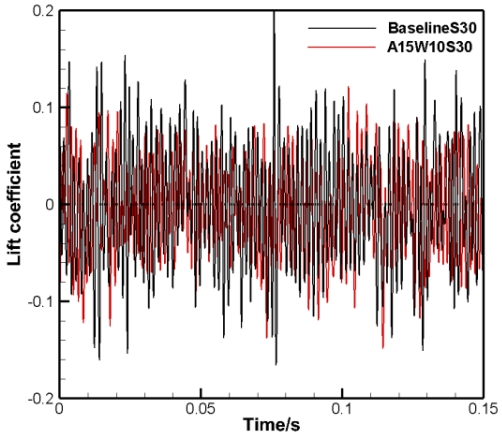

Fig. 6 Time history of airfoil lift and drag coefficient

DOI: 10.13009/EUCASS2019-118

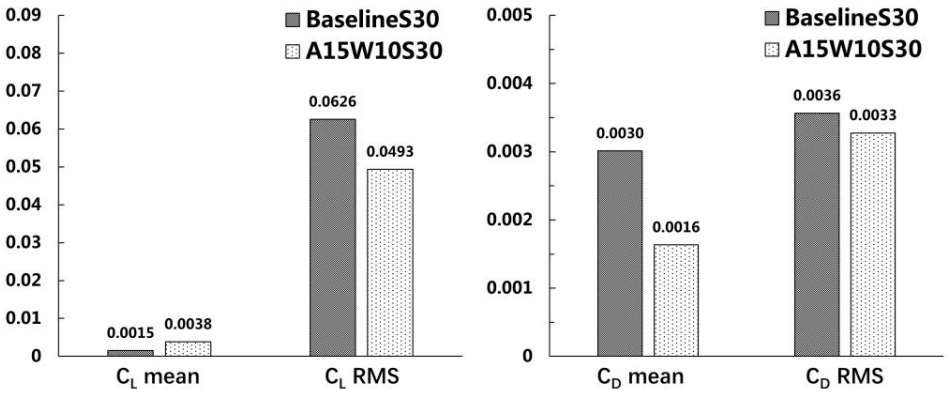

(a) blade lift coefficient

(b) blade drag coefficient

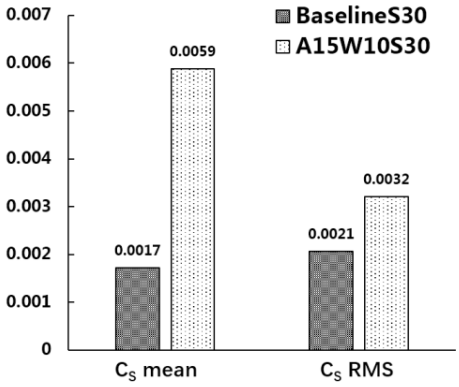

(c) spanwise force coefficient

Fig. 7 Comparison of the mean and RMS value of the airfoil lift, drag and span force coefficient between SLE blade and WLE

Fig. 8 is a comparison of power spectral density(PSD) of fluctuating lift, drag and spanwise forces between the SLE blade and the WLE blade. The frequency of the shedding vortices behand the rod or its primary harmonic frequencies can be observed in these figures. It can be seen from Fig. 8(a) that the characteristic frequency of power spectrum of the fluctuating lift coefficient of the SLE and WLE blade is same as that of the Strouhal number of the shedding vortices behand the rod, which indicates that the lift force fluctuates periodically under the influence of the shedding vortices. The WLE not only reduces the power spectral density of fluctuating lift at the shedding vortices frequency, but also reduces the power spectral density at other broadband frequency ranges. Fig. 8 (b) and Fig. 8(c) indicate that the characteristic frequency of fluctuating drag and spanwise forces is the first harmonic frequency of shedding vortex frequency. This is because the two opposite vortices in Karman vortex street will have the same effect on the drag and spanwise force of the blade when they act on the blade, so that the fluctuation frequency is twice as high as that of the shedding vortices (i.e. the first harmonic frequency). It could be also seen from fig. 8(b) that WLE can also reduce the drag fluctuation in all frequency range. As shown in Fig. 8(c), as expected, the wavy leading edge blade can not only reduce the power spectral density of the spanwise force at the characteristic frequency, but also increase the power spectral density of the spanwise force at all frequencies.

DOI: 10.13009/EUCASS2019-118

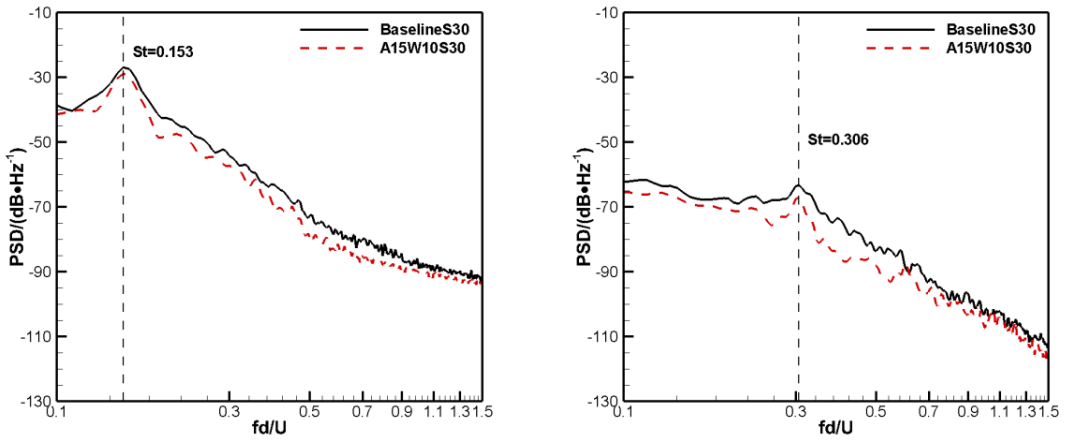

(a) airfoil lift coefficient

(b) airfoil drag coefficient

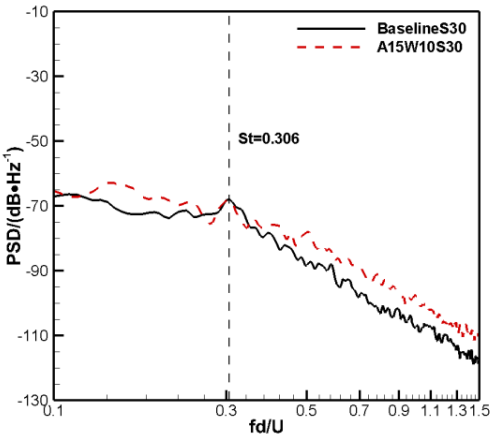

(c) spanwise force coefficient

Fig. 8 Comparison of PSD of the airfoil lift, drag and spanwise force coefficient fluctuation between SLE case and WLE

4.2. Aero-acoustic performance of the swept blade with WLE

Fig. shows the comparison of the aero-acoustic performance between the SLE blade and WLE blade. 9(a) shows the results of sound pressure level at a distance of R=2.0, azimuthal angle of 90° relative to the airfoil center. The azimuthal angle of 0° denotes downstream direction (positive x direction) and 180° denotes upstream direction (negative x direction) and 90° denotes the upside direction relative to the blade surface (positive y direction). It can be found from fig.9(a) that the noise energy is mainly concentrated in the middle and low frequencies close at the characteristic frequencies of Karman Vortex Street. The WLE does not change the characteristic frequency of upstream Karman Vortex Street, nor can it reduce the noise at this characteristic frequency. However, the WLE can reduce the blade-turbulence interaction noise in other frequency. It can be seen from Fig. (a) that wavy LE can significantly reduce the broadband sound pressure level, especially at frequency range of St>0.2.

Fig. (b) shows the results of overall sound pressure level (OASPL) computed from St=0.2 to St=1.5. It could be seen from Fig.9(b) that the directivity of the blade-turbulence interaction noise from swept blade has the "8" shape of the dipole directivity form, the maximum OASPL is presented at the 90° and 270°, while the minimum OASPL is presented at the 0° and 180°. WLE has little effect on the shape of the directivity of the BTI noise. A significant reduction of OASPL at various azimuthal angles is observed. It can be found that the OASPL is reduced about 3.4 dB at 0° and 180°, and OASPL is reduced about 2.4 dB at 90° and 270°. As expected, the reduction of the sound pressure level of BTI noise for three-dimensional swept blade with wavy configuration is not as significant as that of two-dimensional blade. As indicated in previous research work(Tong et al.[35] ,figure 12), for the two-dimensional straight blade, a averaged noise reduction of 9.5 dB with the using of wavy leading edge is observed.

DOI: 10.13009/EUCASS2019-118

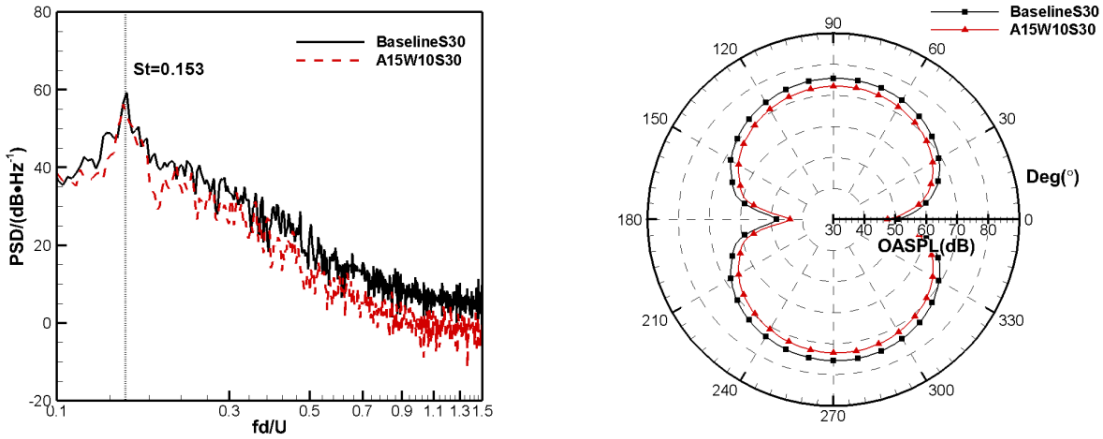

(a) Sound pressure level (at R=2.0m, azimuthal angle of 90°) (b) Overall sound pressure level

Fig. 9 Comparison of the aero-acoustic performance between SLE blade and WLE blade

4.4. Flow field characteristics

The time averaged pressure distribution on the blade surface is displayed in Fig.10 (Because the blade investigated in this study is symmetrical, and the angle of attack of inflow to blade is of 0°, the statistical characteristics of flow field is the same on both sides of the blade). It can be seen from Fig. 2 that the pressure distribution along the spanwise direction is substantially changed due to the wavy leading edge modification. The averaged pressure of the SLE blade is uniformly distributed along the spanwise, and a periodicity of the pressure distribution along the spanwise is observed for the WLE blade with a low pressure region located just downstream of the wavy leading edge valley. It could also be seen that the maximum pressure on leading edge is not at the crest tip, but at the short side of the wave leading edge. This is caused by the impact of the incoming flow on the short side of the wave with the forward direction inflow for swept blade.

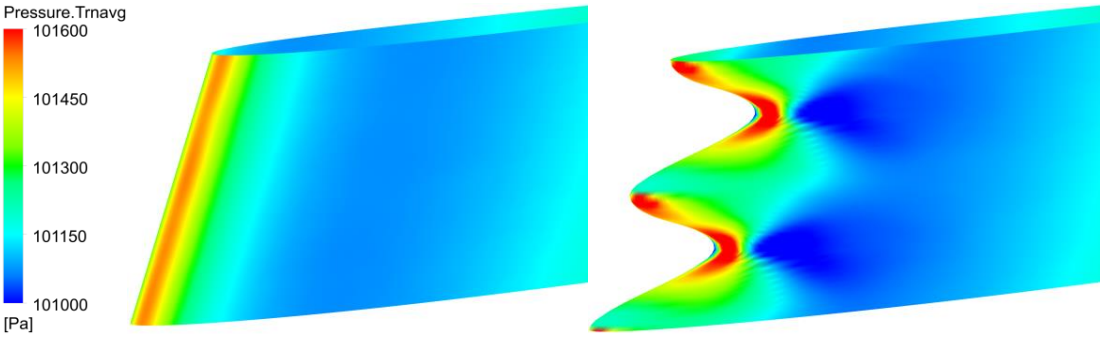

(a)SLE (b) Wavy LE

Fig. 2 Time averaged pressure distribution on the airfoil suction side surface

DOI: 10.13009/EUCASS2019-118

The comparison of time averaged pressure coefficient distribution on the blade is shown in

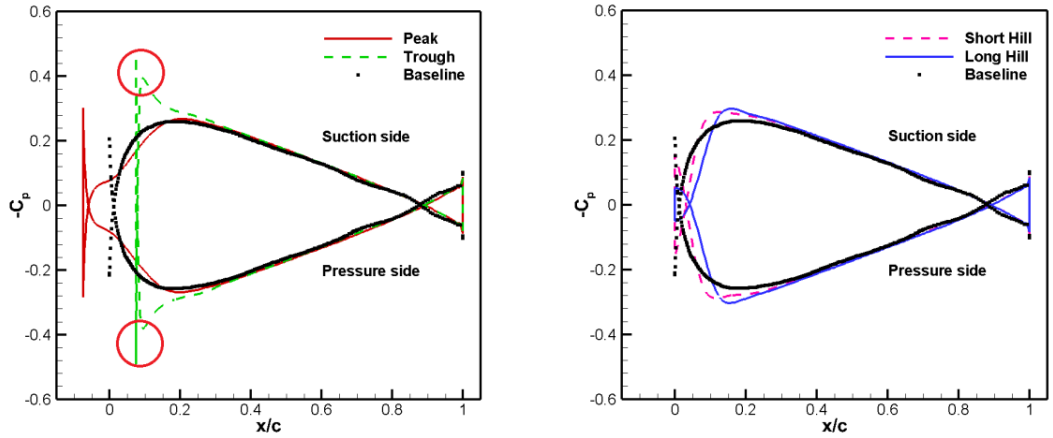

Fig. where the pressure coefficient C_p is defined as

$$C_{\mathrm{p}} = \frac{p - p_0}{\frac{1}{2}\rho_0 U^2} \tag{6}$$

The pressure coefficient distribution of the blade spanwise-section along the wave crest, wave valley and wave hill on both sides of the leading edge of the wave is given in the fig.11. It can be seen from

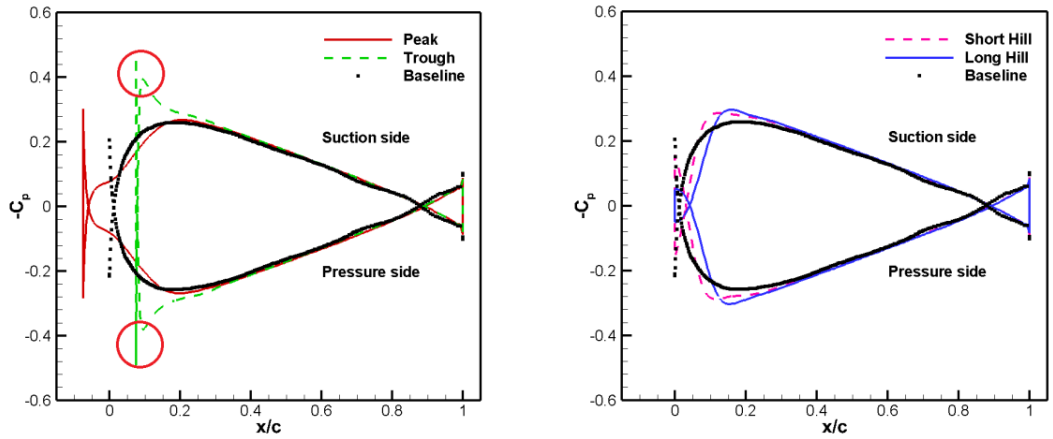

Fig. that WLE has an effect on the pressure coefficient distribution but this effect is limited to the region upstream of x/c=0.3. Downstream of x/c=0.3, the effect of the wavy leading edge on the pressure coefficient is negligible.

For the WLE, the pressure coefficient distribution upstream of x/c=0.3 is different at four different spanwise locations, i.e. peak, valley, short hill and long hill location. An important feature is that the pressure coefficient on the blade surface undergoes more and more sudden change from peak location to valley location. It can be seen that there is a certain pressure gradient along the spanwise direction of the leading edge of WLE blade, which is likely to induce a strong spanwise flow. Moreover, a local minimum of the pressure coefficient is observed behand the wave

DOI: 10.13009/EUCASS2019-118

valley location, which is marked as little red circle region in

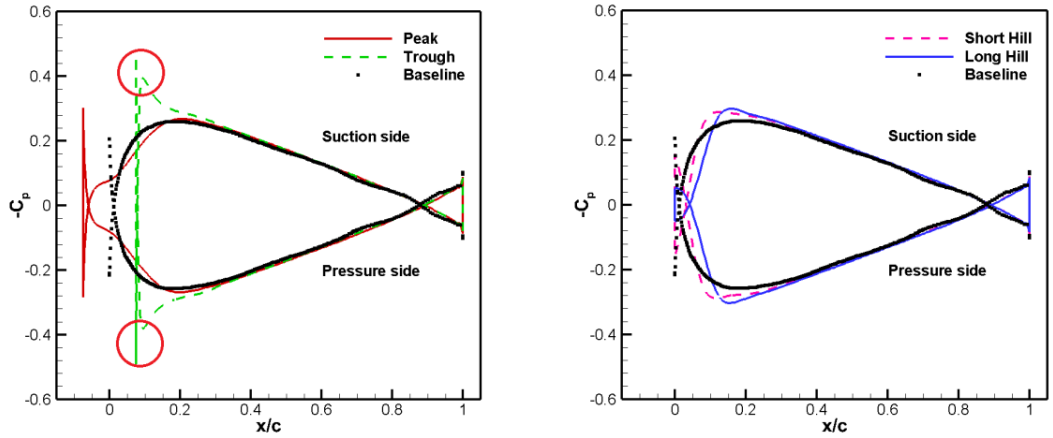

Fig. . It will be shown later that this local minimum of pressure has an impact on the flow characteristics near the leading edge. As shown in the red circle, it can be clearly found that the flow pressure gradient here is very large, and it can be predicted that there must be strong flow characteristics in this region.

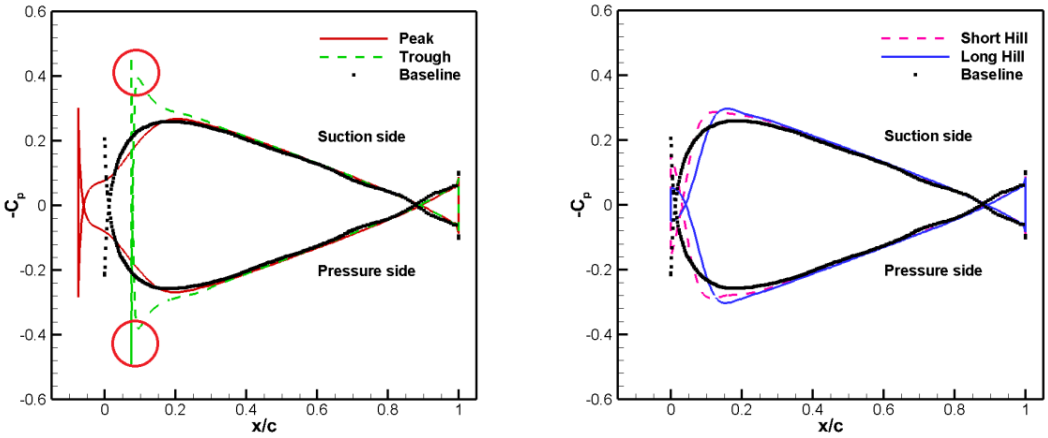

Fig. 11 Time averaged pressure coefficient distribution

Fig. 3 shows the time averaged spanwise component of the wall shear stress distribution along the blade surface for SLE and WLE blade. For the SLE blade, the averaged spanwise component of the wall shear stress is most prominent along the leading edge. Compared with the SLE case, wavy LE blade shows a significant reduction in the averaged wall shear stress along the leading edge, especially around the wavy leading edge long hill location. Downstream of the wave valley, a region of low averaged wall shear stress is observed, as shown in Fig. 3(b).There are positive and negative shear stresses on both sides of the wave valley, and there is a negative shear stress zone at the downstream of the wave valley. These results indicate that there are some transverse secondary flow structures at the wave valley, which have an impact on the shear stress from the leading edge of the blade to the middle region.

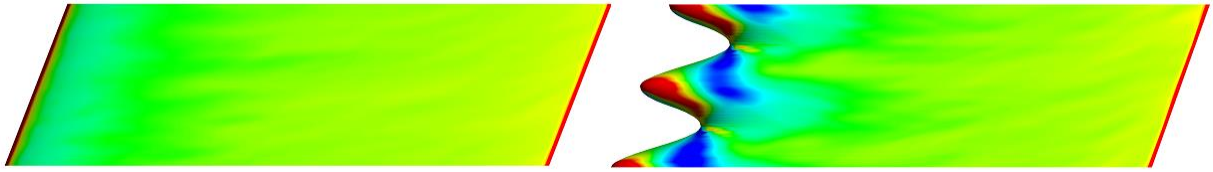

(a)SLE blade (b) WLE blade

Fig. 3 Time averaged spanwise component of wall shear stress distribution

DOI: 10.13009/EUCASS2019-118

Fig. 13 shows the streamwise component of the wall shear stress distribution on the SLE and WLE blade. It can be seen that, for the SLE blade, the streamwise shear stress is uniformly distributed in the spanwise direction, and the streamwise shear stress is the largest at the leading edge. For the WLE blade, the streamwise shear stress is distributed periodically along the spanwise direction. The streamwise shear stress at the crest and valley of the wave is higher than that at other positions, and the streamwise shear stress at the long hill of the wave is lower than that at the short hill. There is a more wide range of low shear stress in the leading edge position for WLE blade. Because streamwise shear stress is closely related to blade friction resistance, it can be expected that the wavy leading edge can effectively reduce the blade resistance.

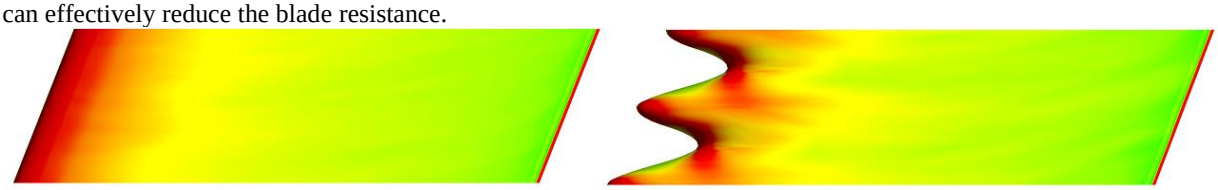

(a)SLE blade (b) WLE blade

Fig. 4 Time averaged streamwise component of wall shear stress distribution

To further investigate the noise reduction mechanism, Fig shows the comparison of wall pressure fluctuation amplitude on blade surface. It can be seen from fig.14 that the pressure fluctuation at the leading edge of the SLE blade is the largest and distributes uniformly along the spanwise direction. This indicats that the leading edge is the main area of pressure fluctuation and the main sound source area. The pressure fluctuation on the WLE blade is the largest in the leading edge area, and it changes periodically along the spanwise direction. The largest pressure fluctuation is on the wave valley position. The pressure fluctuation on the wave crest, short hill and long hill decreases in turn. Compared with the SLE blade, the pressure fluctuation on the WLE blade is larger only in the wave valley position and smaller in the all other position. It could be concluded that the pressure fluctuation of the WLE blade surface is obviously weakened, and the corresponding blade lift and resistance pulsation are reduced. This is one of the main reasons for reducing noise using wavy leading edge.

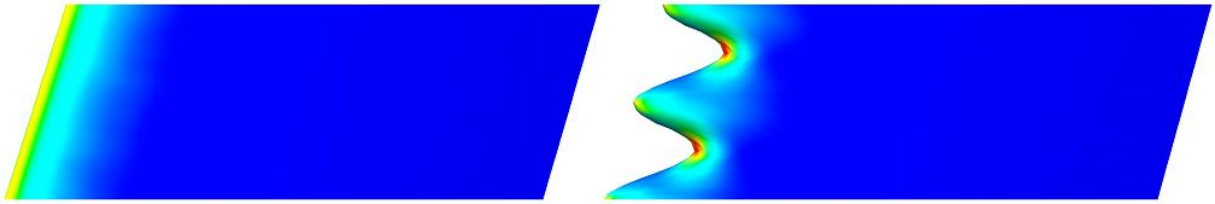

(a) SLE blade (b) WLE blade

Fig.14 Comparison of wall pressure fluctuation amplitude on blade surface

5 Conclusions

A hybrid LES/FW–H acoustic analogy method has been applied to study the effect of wavy leading edge on swept blade-turbulence interaction noise. A rod which is located on the front of a swept blade was used to generated anisotropic turbulence in the inflow to swept blade. The chord of the swept blade is of 150mm and the span is of 300mm.The free-stream speed is of 40m/s with a zero angle of attack and the corresponding blade chord based and rod diameter based Reynolds numbers are about 400,000 and 26,000 respectively. A sinusoidal WLE with amplitude A of 15mm(0.1c) and wavelength W of 10mm(0.67c) is designed to reduce the BTI noise. The main conclusions from this study include:

(1) Wavy leading edge can substantially reduce swept blade lift and drag coefficient fluctuation while the mean lift coefficient does not vary too much. It is found that the fluctuation of lift coefficient and drag coefficient can be reduced by 21.2% and 8.3% respectively in this study. The reduction of lift coefficient and drag coefficient fluctuation indicates that the structure of wavy leading edge can reduce the aerodynamic noise of the swept blade. However, the existence of wavy leading edge can greatly increase the spanwise force on the swept blade, increasing by 247.1%, and at the same time will increase the root mean square value of the spanwise force by about 52.4%.

(2)The wavy leading edge not only reduces the power spectral density of fluctuating lift and drag at the shedding vortices frequency, but also reduces the power spectral density at other broadband frequency ranges. The characteristic frequency of fluctuating drag and spanwise forces is the first harmonic frequency of shedding vortex

frequency. This is because the two opposite vortices in Karman vortex street will have the same effect on the drag and spanwise force of the blade when they act on the blade, so that the fluctuation frequency is twice as high as that of the shedding vortices.

(3) The pressure and shear stress distribution along the spanwise direction is substantially changed due to the WLE modification. There is a more wide range of low shear stress in the leading edge position for WLE blade. Compared with the SLE blade, the pressure fluctuation on the WLE blade is larger only in the wave valley position and smaller in the all other position. It could be concluded that the pressure fluctuation of the WLE blade surface is obviously weakened, and the corresponding blade lift and resistance pulsation are reduced. This is one of the main reasons for reducing noise using wavy leading edge.

(4) The wavy leading edge can substantially reduce BTI noise when the incoming turbulence is anisotropic. The use of wavy leading edge can mitigate noise radiation at all the azimuthal angles without significantly changing the noise directivity. The OASPL of the BTI noise reduction associated with the WLE is approximately 2.4~3.4dB. As expected, the reduction of the sound pressure level of BTI noise for three-dimensional swept blade with WLE configuration is not as significant as that of two-dimensional blade.

Acknowledgement

The present work is supported by the National Natural Science Foundation of China (Grant No. 51776174), the National Special Research Project in Aeroengine in China, the European Union and China collaborative project in aviation - IMAGE project (Contract No. 688971-IMAGE-H2020MG-2014-1015688971). The authors specially wish to acknowledge the IMAGE project. IMAGE (Innovative Methodologies and technologies for reducing Aircraft noise Generation and Emission) is a EU-China collaborative project between the European team (Chalmers, CFDB, CIMNE, KTH, NLR, NUMECA, RWTH-Aachen, ONERA, UPM, VKI, UPM, TU-K and AGI) and Chinese team (ASRI, BUAA, THU, NPU, IMech, BASTRI, ARI, FAI and ACAE). The project is funded by the EC in the H2020 Programme, under Contract No. 688971-IMAGE-H2020-MG-2014-2015 and by the MIIT of China.

References

[1].Oerlemans, S., “Wind Tunnel Aeroacoustic Tests of Six Airfoils for Use on Small Wind Turbines,” Rept. SR-500-35339, NREL, Golden, CO, 2004.

[2].P.T. Soderman, Aerodynamic Effects of Leading-edge Serrations on a Two-dimensional Airfoil, NASA-TM-X-2643, 1972, p. A-3706.

[3].P.T. Soderman, Leading Edge Serrations Which Reduce the Noise of Low-speed Rotors, NASA TN D-7371, 1973.

[4].A.S. Hersh, P.T. Soderman, R.E. Hayden, Investigation of acoustic effects of leading-edge serrations on airfoils, J. Aircraft 11 (4) (1974) 197-202.

[5].Fish, F. E., and Battle, J. M., “Hydrodynamic Design of the Humpback Whale Flipper,” Journal of Morphology, Vol. 225, No. 1, 1995, pp. 51–60. doi:10.1002/(ISSN)1097-4687

[6].Miklosovic, D. S., Murray, M. M., Howle, L. E., and Fish, F. E., “Leading-Edge Tubercles Delay Stall on Humpback Whale (Megaptera Novaeangliae) Flippers,” Physics of Fluids, Vol. 16, No. 5, 2004, pp. L39–L42. doi:10.1063/1.1688341

[7].Miklosovic, D. S., Murray, M. M., and Howle, L. E., “Experimental Evaluation of Sinusoidal Leading Edges,” Journal of Aircraft, Vol. 44, No. 4, 2007, pp. 1404–1408. doi:10.2514/1.30303

[8].Johari, H., Henoch, C., Custodio, D., and Levshin, A., “Effects of Leading-Edge Protuberances on Airfoil Performance,” AIAA Journal, Vol. 45, No. 11, 2007, pp. 2634–2642. doi:10.2514/1.28497

[9].Stanway, M. J., “Hydrodynamic Effects of Leading-Edge Tubercles on Control Surfaces and in Flapping Foil Propulsion,” Ph.D. Dissertation, Massachusetts Inst. of Technology, Cambridge, MA, 2008. [10] Van Nierop, E., Alben, S., and Brenner, M., “How Bumps on Whale Flippers Delay Stall: An Aerodynamic Model,” Physical Review

[10]. Letters, Vol. 100, No. 5, 2008, pp. 1–4. doi:10.1103/PhysRevLett.100.054502

[11]. Pedro, H. T. C., and Kobayashi, M. H., “Numerical Study of Stall Delay on Humpback Whale Flippers,” 46th AIAA Aerospace Sciences Meeting and Exhibit, AIAA Paper 2008-584, 2008.

[12]. Hansen, K. L., Kelso, R. M., and Dally, B. B., “Performance Variations of Leading-Edge Tubercles for Distinct Airfoil Profiles,” AIAA Journal, Vol. 49, No. 1, 2011, pp. 185–194. doi:10.2514/1.J050631

[13]. Yoon, H. S., Hung, P. A., Jung, J. H., and Kim, M. C., “Effect of the Wavy Leading Edge on Hydrodynamic Characteristics for Flow Around Low Aspect RatioWing,” Computers and Fluids, Vol. 49, No. 1, 2011, pp. 276–289. doi:10.1016/j.compfluid.2011.06.010

[14]. Weber, P. W., Howle, L. E., Murray, M. M., and Miklosovic, D. S., "Computational Evaluation of the Performance of Lifting Surfaces with Leading-Edge Protuberances," Journal of Aircraft,Vol. 48, No. 2, 2011, pp. 591–600. doi:10.2514/1.C031163
[15]. Favier, J., Pinelli, A., and Piomelli, U., "Control of the Separated Flow Around an Airfoil Using aWavy Leading Edge Inspired by Humpback Whale Flippers," Comptes Rendus Mecanique, Vol. 340, Nos. 1–2, 2012, pp. 107–114. doi:10.1016/j.crme.2011.11.004
[16]. Zhang, M. M., Wang, G. F., and Xu, J. Z., "Aerodynamic Control of Low-Reynolds-Number Airfoil with Leading-Edge Protuberances," AIAA Journal, Vol. 51, No. 8, 2013, pp. 1960–1971. doi:10.2514/1.J052319
[17]. Zhang, X.W., Zhou, C.Y., Zhang, T., and Ji,W. T., "Numerical Study on Effect of Leading-Edge Tubercles," Aircraft Engineering and Aerospace Technology, Vol. 85, No. 4, 2013, pp. 247–257. doi:10.1108/AEAT-Feb-2012-0027
[18]. Karthikeyan, N., Sudhakar, S., and Suriyanarayanan, P., "Experimental Studies on the Effect of Leading Edge Tubercles on Laminar Separation Bubble," 52nd Aerospace Sciences Meeting, AIAA Paper 2014-1279,2014.
[19]. V. Clair, C. Polacsek, T. Le Garrec, G. Reboul, M. Gruber, P. Joseph, Experimental and numerical investigation of turbulence-airfoil noise reduction using wavy edges, AIAA J. 51 (11) (2013) 2695e2713.
[20]. A.S.H. Lau, S. Haeri, J.W. Kim, The effect of wavy leading edges on aerofoil-gust interaction noise, J. Sound Vib. 332 (24) (2013) 6234e6253.
[21]. T.P. Chong, A. Vathylakis, A. McEwen, F. Kemsley, C. Muhammad, S. Siddiqi, Aeroacoustic and aerodynamic performances of an aerofoil subjected to sinusoidal leading edges, in: 21st AIAA/CEAS Aeroacoustics Conference, Dallas, June 2015. AIAA paper 2015e2200.
[22]. S. Narayanan, P. Chaitanya, S. Haeri, P. Joseph, J.W. Kim, C. Polacsek, Airfoil noise reductions through leading edge serrations, Phys. Fluids 27 (2) (2015) 25109e25117.
[23]. P. Chaitanya, S. Narayanan, P. Joseph, C. Vanderwel, J. Turner, Broadband noise reduction through leading edge serrations on realistic aerofoils, in: 21st AIAA/CEAS Aeroacoustics Conference,Dallas, June 2015. AIAA paper 2015e2202.
[24]. J.W. Kim, S. Haeri, P.F. Joseph, On the reduction of aerofoil-turbulence interaction noise associated with wavy leading edges, J. Fluid Mech. 792 (2016) 526e552.
[25]. J. Mathews, N. Peake, Noise generation by turbulence interacting with an aerofoil with a serrated leading edge, in: 21st AIAA/CEAS Aeroacoustics Conference, Dallas, June 2015. AIAA Paper 2015e2204.
[26]. B. Lyu, M. Azarpeyvand, S. Sinayoko, Noise prediction for serrated leading-edges, in: 22nd AIAA/CEAS Aeroacoustics Conference, Lyon, France, May 2016. AIAA Paper 2016e2740.
[27]. P. Chaitanya, P. Joseph, S. Narayanan, C. Vanderwel, J. Turner, J.W. Kim, B. Ganapathisubramani, Performance and mechanism of sinusoidal leading edge serrations for the reduction of turbulenceeaerofoil interaction noise, J. Fluid Mech. 818 (2017) 435e464.
[28]. T.M. Biedermann, T.P. Chong, F. Kameier, C.O. Paschereit, Statisticaleempirical modeling of airfoil noise subjected to leading-edge serrations, AIAA J. 55 (9) (2017) 3128e3142.
[29]. J.M. Turner, J.W. Kim, Aeroacoustic source mechanisms of a wavy leading edge undergoing vortical disturbances, J. Fluid Mech. 811 (2017) 582e611.
[30]. F.G. Aguilera, J. Gill, D. Angland, X. Zhang, Wavy leading edge airfoils interacting with anisotropic turbulence, in: 23rd AIAA/CEAS Aeroacoustics Conference, Denver, Colorado, 5-9 June 2017. AIAA paper 2017e3370.
[31]. G. Reboul, A. Cader, C. Polacsek, T.L. Garrec, R. Barrier, N.B. Nasr, CAA prediction of rotor-stator interaction using synthetic turbulence: application to a low-noise serrated OGV, in: 23rd AIAA/CEAS Aeroacoustics Conference, Denver, Colorado, 5-9 June 2017. AIAA paper 2017e3714.
[32]. W.J. Chen, X.N. Wang, W.Y. Qiao, L.F. Wang, F. Tong, Rod-airfoil interaction noise reduction using leading edge serrations, in: 21st AIAA/CEAS Aeroacoustics Conference,, Dallas, TX, 22-26 June 2015. AIAA paper 2015-3264.
[33]. Weijie Chen, Weiyang Qiao, Fan Tong, Liangfeng Wang, Xunnian Wang. Experimental investigation of wavy leading edges on rod-aerofoil interaction noise. Journal of Sound and Vibration, 422, 2018: 409-431.
[34]. Weijie Chen, Weiyang Qiao, Fan Tong, Liangfeng Wang, Xunnian Wang. Numerical investigation of wavy leading edges on rod-airfoil interaction noise. AIAA Journal, 56(7), 2018: 2553-2567.
[35]. Fan TONG,Weiyang QIAO,Weijie CHEN,Haoyi CHENG,Renke WEI,Xunnian WANG.Numerical analysis of broadband noise reduction with wavy leading edge[J].Chinese Journal of Aeronautics,2018,31(07):1489-1505.
[36]. Turner JM, Kim JW. Aeroacoustic source mechanisms of a wavy leading edge undergoing vortical disturbances. J Fluid Mech, 2017;811(1):582–611.
[37]. Fan Tong, Weiyang Qiao, Kunbo Xu, Liangfeng Wang, Weijie Chen, Xunnian Wang. On the study of wavy leading-edge vanes to achieve low fan interaction noise [J]. Journal of Sound and Vibration, 2018, 419:200-226.

[38]. G. Reboul, A. Cader, C. Polacsek, T.L. Garrec, R. Barrier, N.B. Nasr, CAA prediction of rotor-stator interaction using synthetic turbulence: application to a low-noise serrated OGV, in: 23rd AIAA/CEAS Aeroacoustics Conference, Denver, Colorado, 5-9 June 2017. AIAA paper 2017e3714.
[39]. Fan Tong, Weiyang Qiao, Weijie Chen, Liangfeng Wang, Xunnian Wang, Broadband noise prediction using large eddy simulation and a frequency domain method [J]. Applied Acoustics, 2017,117: 94–105.
[40]. Wagner CD, Hüttl T, Sagaut P. Large-eddy simulation for acoustics. 1st edition. Cambridge : Cambridge University Press; 2012. p. 90.
[41]. ANSYS CFX. Reference guide, release 14.0. ANSYS Inc.; 2011.
[42]. Germano M, Piomelli U, Moin P, et al. A dynamic subgrid-scale eddy viscosity model. Physics of Fluids 1991; A3 (7): 1760-1765.
[43]. Winkler J, Moreau S, Carolus T. Large-eddy simulation and trailing-edge noise prediction of an airfoil with boundary-layer tripping. AIAA-2009-3197, 2009.
[44]. Goldstein ME. Unified approach to aerodynamic sound generation in the presence of solid boundaries. J Acoust Soc Am 1974;56:497–509.
[45]. Boudet, J.,Grosjean, N., and Jacob,M. C., "Wake-Airfoil Interaction as Broadband Noise Source: A Large-Eddy Simulation Study," International Journal of Aeroacoustics, Vol. 4, Nos. 1–2, 2005, pp. 93–115. doi:10.1260/1475472053730093
[46]. Kato, C., Lida, A., Takano, Y., Fujita, H., and Ikegawa, M., "Numerical Prediction of Aerodynamic Noise Radiated from Low Mach Number Turbulent Wake," 31st Aerospace Sciences Meeting & Exhibit, AIAA Paper 1993-0145, 1993.